Classical model emerges in quantum entanglement: Quantum Monte Carlo study for an Ising-Heisenberg bilayer

Siying Wu [1,2,*] Xiaoxue Ran [3,*] Binbin Yin [4] Qi-Fang Li,[5] Bin-Bin Mao,[6,†] Yan-Cheng Wang,[2,‡] and Zheng Yan[7,8,3,§]

[1]*State Key Laboratory of Surface Physics and Department of Physics, Fudan University, Shanghai 200438, China*

[2]*Beihang Hangzhou Innovation Institute Yuhang, Hangzhou 310023, China*

[3]*Department of Physics and HKU-UCAS Joint Institute of Theoretical and Computational Physics, The University of Hong Kong, Pokfulam Road, Hong Kong SAR, China*

[4]*Department of Architecture and Civil Engineering, City University of Hong Kong, Kowloon, Hong Kong, China*

[5]*The Institute for Solid State Physics, The University of Tokyo, Chiba 277-8581, Japan*

[6]*School of Foundational Education, University of Health and Rehabilitation Sciences, Qingdao 266071, China*

[7]*Department of Physics, School of Science, Westlake University, 600 Dunyu Road, Hangzhou 310030, Zhejiang Province, China*

[8]*Institute of Natural Sciences, Westlake Institute for Advanced Study, 18 Shilongshan Road, Hangzhou 310024, Zhejiang Province, China*

(Received 27 June 2022; revised 12 October 2022; accepted 22 March 2023; published 10 April 2023)

By developing a cluster sampling of the stochastic series expansion quantum Monte Carlo method, we investigate a spin-$\frac{1}{2}$ model on a bilayer square lattice with intralayer ferromagnetic (FM) Ising coupling and interlayer antiferromagnetic Heisenberg interaction. The continuous quantum phase transition which occurs at $g_c = 3.045(2)$ between the FM Ising phase and the dimerized phase is studied via large-scale simulations. From analysis of the critical exponents we show that this phase transition belongs to the (2+1)-dimensional Ising universality class. In addition, the quantum entanglement is strong between the two layers, especially in the dimerized phase. The effective Hamiltonian of a single layer seems like a transverse-field Ising model. However, we found that the quantum entanglement Hamiltonian is a pure classical Ising model without any quantum fluctuations. Furthermore, we give a more general explanation about how a classical entanglement Hamiltonian emerges.

DOI: 10.1103/PhysRevB.107.155121

I. INTRODUCTION

Quantum entanglement is a powerful tool to detect and characterize the informational, field-theoretical, and topological properties of quantum many-body states [1–4], which combines the conformal field theory (CFT) and the categorial description of the problem [5–17]. Since Li and Haldane pointed out that the entanglement spectrum (ES) is an important measurement with more information than the entanglement entropy (EE) [18–20], a low-lying ES has been widely employed as a fingerprint of CFT and topology [21–37]. The entanglement Hamiltonian (EH) $\mathcal{H}_A = -\ln(\rho_A)$ can be obtained from the reduced density matrix (RDM) $\rho_A = \mathrm{Tr}_B(\rho)$ of the system A by tracing out the environment B [18,38]. The energy spectrum of the entanglement Hamiltonian $\mathcal{H}_A$, which is usually called the entanglement spectrum, describes the rich information of the system A.

Most of the numerical studies of ES have focused on (quasi-)one-dimensional [(quasi-)1D] systems so far, because of the limitations of the numerical methods. For example, due to the exponential growth of the computational complexity and memory cost, numerical methods such as exact diagonalization (ED) and the density matrix renormalization group (DMRG) have therefore obvious limitations for an entangling region with long boundaries of the lattice and higher dimensions. Recently, a novel scheme has been proposed to extract the information of a high-dimensional entanglement spectrum by using the quantum Monte Carlo (QMC) method, which opens a new way to study the ES and EH of many-body systems [39].

An interesting question can be asked: Can the EH, which is used to describe quantum entanglement, be a classical model (e.g., an Ising model)? Intuitively, the two are contradictory. For example, all the eigenstates (as well as the ground state) of the Ising model are classical direct-product states without any entanglement. However, the EH itself is different from the original Hamiltonian, and we cannot exclude the possibility that this seemingly contradictory situation actually occurs. In fact, such an example has been successfully constructed in this paper on a bilayer lattice, and the result is not limited to this case according to our discussion. The bilayer lattice can be divided into two 2D layer parts, which is well suited for studying the 2D entanglement properties. As the simplest layered structure, it has revealed many novel physical phenomena in 2D systems [40–57]. To answer the above question, we design a bilayer model in which each spin in the system (the first layer) is coupled to the environment (the second layer) with antiferromagnetic (AFM) Heisenberg interaction which introduces entanglement between the two layers. This

*These authors contributed equally to this work.
†maobinbin@uor.edu.cn
‡wangyancheng@zfau.cn
§zhengyan@westlake.edu.cn

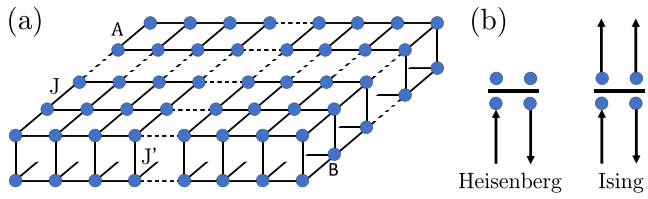

FIG. 1. (a) Spin-$\frac{1}{2}$ bilayer model on an $L \times L$ square lattice. L is the length of each layer. J is the nearest-neighbor intralayer ferromagnetic Ising interaction, and J' is the interlayer antiferromagnetic Heisenberg interaction. (b) Schematic diagram of update lines on the space-time lattice, where the horizontal line represents the diagonal or off-diagonal operator and above and below the line are four legs of a vertex. When the update line meets a Heisenberg operator, only the neighbor leg of the initial leg creates an update line (left panel). In contrast, all the other three vertex legs create update lines when the update line meets an Ising operator (right panel).

bilayer model with spin $\frac{1}{2}$ is defined on an $L \times L$ square lattice with intralayer ferromagnetic (FM) Ising interaction and interlayer AFM Heisenberg interaction, as shown in Fig. 1(a). The Hamiltonian is given by

$$H = -J \sum_{\langle i,j \rangle} \left(S^z_{A,i} S^z_{A,j} + S^z_{B,i} S^z_{B,j} \right) + J' \sum_i S_{A,i} S_{B,i}, \qquad (1)$$

where $S_{A,i}$ and $S_{B,i}$ are spin operators at site i of the A (upper) and B (bottom) layers, while S^z represents the spin operator along the z axis. $\langle i, j \rangle$ denotes a pair of the nearest-neighbor sites on the same layer with periodic boundary conditions. $J(> 0)$ is the intralayer Ising coupling strength, and $J'(> 0)$ is the interlayer Heisenberg interaction.

In this paper, we develop a highly efficient cluster update scheme of the stochastic series expansion (SSE) QMC algorithm (Sec. II) and investigate the ground-state phase diagram of the spin-$\frac{1}{2}$ bilayer model (Sec. III). The transition point and the critical exponents obtained from QMC simulations demonstrate that this continuous quantum phase transition (QPT) belongs to the 3D Ising universality class. Then we measure the imaginary time correlations of the EH by a newly developed QMC method [39] to prove that the EH is always diagonal in the whole region of the phase diagram. We give an argument to explain how the quantum model can emerge as a classical EH in Sec. IV and a conclusion in Sec. V.

II. METHOD

In this section, we will introduce our efficient update scheme within the SSE frame to deal with the Heisenberg-Ising mixed interactions. Readers who are not interested in the algorithm can skip to the next section; it does not affect the physical results. Although the conventional directed-loop SSE algorithm [58,59] can be employed to solve a model which contains both Ising and Heisenberg interactions, we found that it does not work effectively due to the pure Ising interaction. Therefore we have developed a cluster method based on SSE combining the operator loop updates for the Heisenberg model [60,61] and cluster updates for the transverse-field Ising model [62]. Details of the algorithm are explained below. We note that readers who are not familiar with the SSE may need a detailed SSE tutorial [63] to learn more basics.

In the SSE QMC method, the partition function can be written as [60,61]

$$\begin{aligned} Z &= \mathrm{Tr}\{e^{-\beta H}\} \\ &= \sum_\alpha \sum_{S_M} (-1)^{n_2} \frac{\beta^n (M-n)!}{M!} \left\langle \alpha \left| \prod_{p=0}^{M-1} H_{a(p),b(p)} \right| \alpha \right\rangle, \end{aligned} \qquad (2)$$

where α sum over all states in the system, S_M denotes the strings of the bond operators, and M is the series expansion cutoff. n is the total number of the operators, and n_2 is the number of off-diagonal operators. β is the inverse temperature. Firstly, we add the constant $\frac{1}{4}$ into the Hamiltonian to avoid the sign problem, as we usually do in SSE [60,61,64,65], and separate it into the Ising part (H_I) and the Heisenberg part (H_H):

$$\begin{aligned} H &= -\sum_{\langle ij \rangle} H_I - \sum_i H_H, \\ H_I &= J \left[\left(S^z_{A,i} S^z_{A,j} + \frac{1}{4} \right) + \left(S^z_{B,i} S^z_{B,j} + \frac{1}{4} \right) \right], \\ H_H &= H_{1,H} + H_{2,H} \\ &= J' \left[\left(\frac{1}{4} - S^z_{A,i} S^z_{B,i} \right) + \frac{1}{2} (S^+_{A,i} S^-_{B,i} + S^-_{A,i} S^+_{B,i}) \right], \end{aligned} \qquad (3)$$

where H_I is the diagonal operator as well as $H_{1,H} = J'(\frac{1}{4} - S^z_{A,i} S^z_{B,i})$, and $H_{2,H} = \frac{J'}{2}(S^+_{A,i} S^-_{B,i} + S^-_{A,i} S^+_{B,i})$ is the off-diagonal operator. Taking S^z as a complete set of basis for the system, the nonzero matrix elements are

$$\begin{aligned} \langle \uparrow\uparrow | H_I | \uparrow\uparrow \rangle &= \langle \downarrow\downarrow | H_I | \downarrow\downarrow \rangle = \frac{J}{2}, \\ \langle \uparrow\downarrow | H_{1,H} | \uparrow\downarrow \rangle &= \langle \downarrow\uparrow | H_{1,H} | \downarrow\uparrow \rangle = \frac{J'}{2}, \\ \langle \uparrow\downarrow | H_{2,H} | \downarrow\uparrow \rangle &= \langle \downarrow\uparrow | H_{2,H} | \uparrow\downarrow \rangle = \frac{J'}{2}. \end{aligned} \qquad (4)$$

The sampling procedures include the diagonal updates and the cluster updates. The diagonal updates either insert or remove a diagonal operator between two states with acceptance probabilities, which are regulated by the detailed balanced condition. The cluster updates change the types of operators by flipping all spins on the clusters with probability $\frac{1}{2}$.

We describe the updating scheme in the following steps.

A. Diagonal update

We go through the operator strings along the imaginary time direction and either remove or insert a diagonal operator on a randomly selected bond. If the chosen bond has two parallel (antiparallel) spins on its endpoints, the insertion of the Heisenberg (Ising) operator is forbidden. So, we will have several conditions.

Condition (a). For a diagonal operator (H_I or $H_{1,H}$), we removed it with the acceptance probability

$$P_{\text{remove}} = \min \left(\frac{M-n+1}{\beta(N_H J' + 2N_I J)/2}, 1 \right), \qquad (5)$$

where N_H is the number of interlayer bonds, N_I is the number of intralayer bonds in each layer, and thus $N_I = 2N_H$ according to our definition.

Condition (b). For a null operator, we substitute it with a diagonal operator H_I or $H_{1,H}$ by the procedures below.

(i) Firstly, we decide which type of diagonal operators to insert. We choose to insert H_I with probability

$$P(I) = \frac{2N_I J}{N_H J' + 2N_I J} \tag{6}$$

or H_H with probability $P(H) = 1 - P(I)$.

(ii) Once the decision has been made, we need to choose a certain position for the operator with probability $1/N_H$ or $1/2N_I$. Then the operator will be inserted with the acceptance probability

$$P_{\text{insert}} = \min\left(\frac{\beta(N_H J' + 2N_I J)/2}{M - n}, 1\right). \tag{7}$$

Condition (c). For an off-diagonal operator, we ignore it and go to the next slice of imaginary time.

B. Cluster update

(a) A schematic diagram of update lines in the configuration space is shown in Fig. 1(b). The QMC method is based on the path integral in imaginary time [58,66,67]. The evolution of the system can be mapped on the space-time lattice. For each step of the imaginary time propagation, an operator acts on the initial state, and a new propagated state is obtained. Figure 1(b) shows the action of the operator, where the horizontal line represents the diagonal or off-diagonal operator, and above and below the line are four legs of a vertex. When an update line meets an Ising operator (intralayer), all the other three vertex legs create update lines. In contrast, only the neighbor leg of the initial leg creates an update line when an update line meets a Heisenberg operator (interlayer).

For the off-diagonal updates, we follow two rules to construct the clusters: (1) The two neighbor legs on the same side of a Heisenberg operator H_H belong to the same cluster, and (2) the four legs of a Ising operator H_I belong to one cluster. In this way, the update line evolves and forms a cluster eventually.

(b) Then the clusters constructed from the above rules are flipped with probability $\frac{1}{2}$, which is according to the Swendsen-Wang cluster updating scheme.

C. Remark

All the details about the update acceptance probability are similar to the previous SSE: The update of Heisenberg operators obeys the operator loop method for the Heisenberg model [60,61], and that of Ising operators obeys the cluster updates for the transverse-field Ising model [62,68–70].

III. PHASE DIAGRAM AND CRITICAL EXPONENTS

Using the QMC method we developed for the spin-$\frac{1}{2}$ bilayer model, we study the ground states and the critical properties of the system. Here we set the coupling ratio $g = J'/J$. When $g \to 0$, the intralayer FM Ising coupling J dominates, and the system favors a FM phase where all the spins in the same layer are parallel. When $g \to \infty$, which means that the interlayer AFM Heisenberg interaction J' is very large, the state corresponds to a dimerized phase where the two spins of different layers are coupled into a singlet. The phase diagram of the system is shown in Fig. 2.

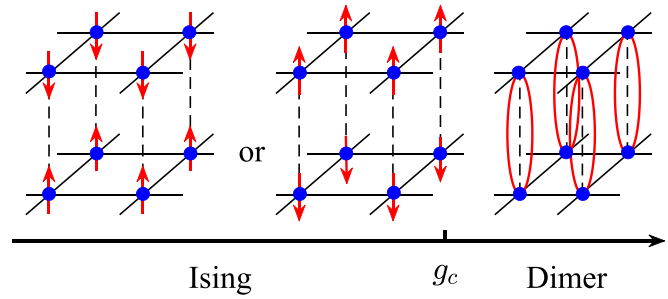

FIG. 2. Ground-state phase diagram of the square-lattice bilayer model. When $g > g_c$, there is a twofold degenerate FM phase, where spins in the same layer are aligned parallel. For $g > g_c$, the ground state corresponds to a dimerized phase where spins in different layers couple into singlets.

To further understand the phase transition in this system, we calculated several physical observables, including the order parameter m, the Binder cumulant U_2, the susceptibility χ, and the spin-spin correlation function $G(r)$. The order parameter m is defined as the magnetization difference between the top and bottom layers:

$$m = \sum_i \left(S^z_{A,i} - S^z_{B,i}\right). \tag{8}$$

The Binder cumulant [71,72] U_2 is given by

$$U_2 = \tfrac{3}{2}\left(1 - \tfrac{1}{3}R_2\right), \tag{9}$$

where $R_2 = \langle m^4\rangle/\langle m^2\rangle^2$ is the Binder ratio [71,73] of the order parameter m. The susceptibility χ can be expressed as

$$\chi = \frac{\beta}{N}(\langle m^2\rangle - \langle|m|\rangle^2), \tag{10}$$

where N is the total number of spins. The spin-spin correlation function $G(r)$ can be written as

$$G(r) = \left\langle S^z_0 S^z_r\right\rangle, \tag{11}$$

where r is the distance between two sites.

The order parameter m versus g for different system sizes is shown in Fig. 3(a), which depicts the vanishing of the FM phase. As g increases, $\langle|m|\rangle$ tends toward zero, where two spins in different layers form a singlet. To study the phase transition between the FM state and the dimerized phase, we show a log-log plot of $\langle|m|\rangle$ in Fig. 3(b) to analyze its different decay behaviors in different phases. We found that in the FM phase ($g < g_c$), $\langle|m|\rangle$ drops to a constant as the system size increases. In contrast, in the dimerized phase ($g > g_c$), the order parameter exponentially decays to 0 as $L \to \infty$. At the critical point g_c, $\langle|m|\rangle$ shows a nontrivial power-law decay.

To determine the critical point g_c, we obtain the Binder cumulant and its data collapse with 3D Ising critical exponents, which are shown in Fig. 4. We calculate systems with $L = 8, 16, 24, 32$. The drift of the crossing points of different system sizes in Fig. 4(a) indicates the finite-size effect in

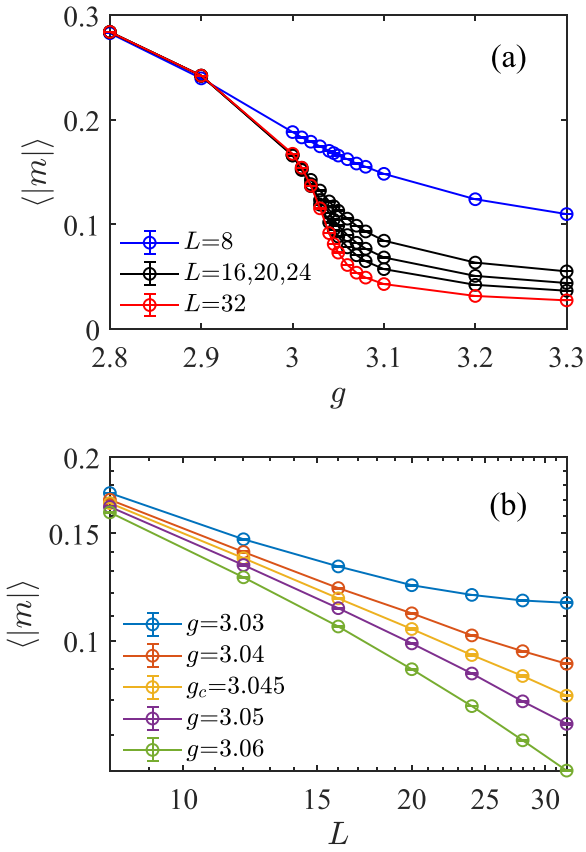

FIG. 3. (a) The order parameter m as a function of the coupling ratio g. As g increases, $\langle|m|\rangle$ eventually decays to zero indicating the vanishing of the FM phase. We calculate data with a smaller interval nearby the critical point to illustrate the continuous quantum phase transition in the system. (b) Log-log plot of $\langle|m|\rangle$ around the transition point g_c. We find that in the FM phase the order parameter decays to a constant, while it decays to 0 in the dimerized phase. At the critical point, it shows a power-law decay.

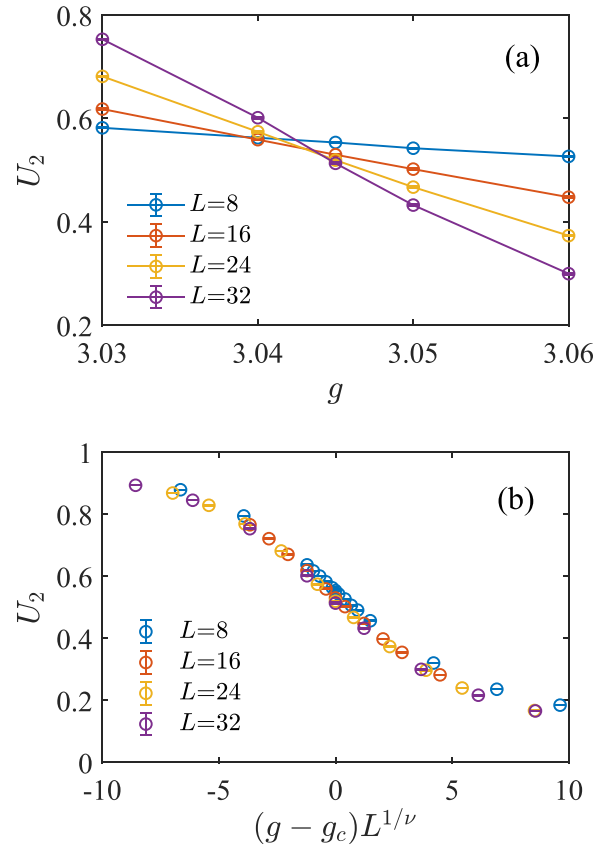

FIG. 4. (a) The Binder cumulant U_2 vs g. We determine the critical point g_c by extrapolating the crossing points of U_2 curves with different system sizes, which gives $g_c = 3.045(2)$. (b) The high-quality data collapse of the Binder cumulant at the critical point. Here we use the 3D Ising critical exponent $\nu = 0.63$ in the scaling, which suggests that our numerical results satisfy the 3D Ising universality class.

the system. So we perform an extrapolation of these crossing points to obtain the critical point in the thermodynamic limit, which gives $g_c = 3.045(2)$. The high-quality data collapse of U_2 in Fig. 4(b), where $\nu = 0.63$ is the 3D Ising critical exponent [74,75], suggests that the FM-phase-to-dimerized-phase transition belongs to the 3D Ising universality class.

Besides, the susceptibility χ illustrated in the Fig. 5 shows a peak in the transition point, which is supposed to diverge with increasing system size L. Data with a smaller interval are calculated to show the peak more clearly. We also perform the data collapse according to the scaling law $\tilde{\chi}(L,t) = L^{-\gamma/\nu}\chi(tL^{1/\nu})$ [76]. Here, we use the Ising critical exponents ν and γ, where $\gamma = 1.24$. The data collapse is very good near the critical point.

We also consider the equal-time spin-spin correlation function $G(r)$ of a single layer, which is shown in Fig. 6 in a log-log plot. At the critical point, $G(r)$ should decay as a power law $G(r) \sim r^{-(1+\eta)}$. As a comparison, we plot the $\eta = 0.036$ line of the 3D Ising universality. These pieces of numerical evidence confirm that there is a 3D Ising transition between the FM phase and the dimerized phase.

IV. ENTANGLEMENT HAMILTONIAN

The Heisenberg interactions favor binding the spins of different layers into singlets and induce the quantum entanglement between two layers. Obviously, the strength of the quantum entanglement between layer A and layer B should be different in FM and dimerized phases. We try to extract the information of the EH from QMC simulation through a recently developed method which gained the ES successfully [39]. According to this method, we can obtain the imaginary time correlations of the entanglement Hamiltonian $H_A = -\ln(\rho_A)$ via constructing the replica manifold to simulate $\mathrm{Tr}(\rho_A^n)$. Here, $\rho_A = \mathrm{Tr}_B(\rho)$ is the RDM of layer A, and ρ is the density matrix of the bilayer system. The key point of this method is that the imaginary time correlation function can be obtained by simulating $\mathrm{Tr}(\rho_A^n)$ via the QMC method [34–36,39]. Therefore, if we treat the n as the inverse temperature β for the entanglement Hamiltonian H_A, every $\rho_A = e^{-H_A}$ can be seen as an imaginary time evolution operator with the time length 1.

We now discuss the S^z imaginary time correlations of the EH, i.e., $G(\tau) = \langle S^z(\tau)S^z(0)\rangle_{\mathrm{EH}}$. It is interesting that we find that $G(\tau)$ does not decay regardless of the phase of the system.

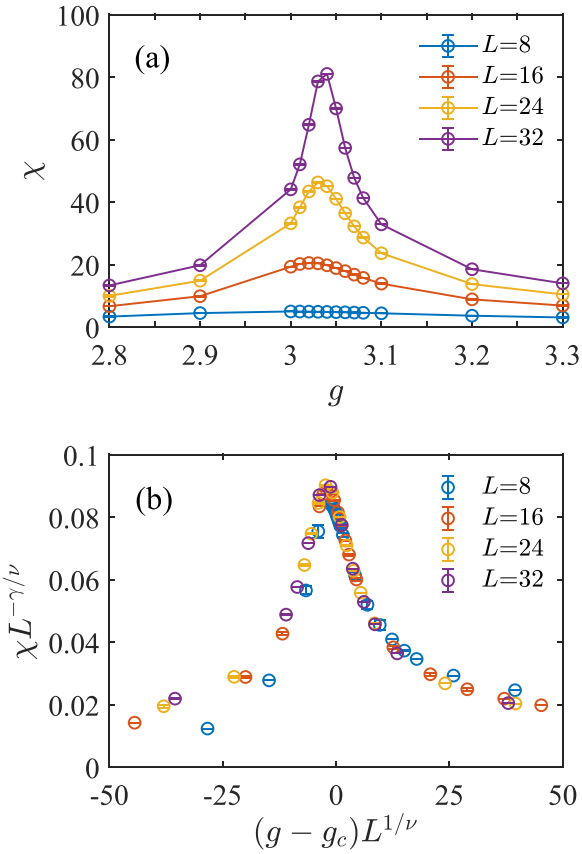

FIG. 5. (a) The susceptibility χ as a function of g. The peak in the critical point diverges as the system size L increases. (b) The data collapse of the susceptibility is observed with 3D Ising exponents $\nu = 0.63$ and $\gamma = 1.24$, and our prediction for the universality class is confirmed again.

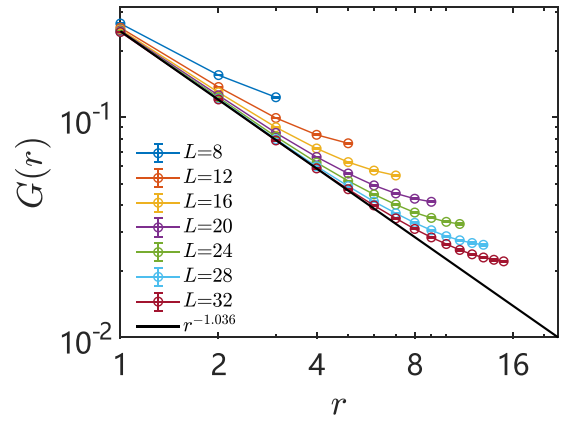

FIG. 6. Log-log plot of the equal-time spin-spin correlation function $G(r)$ vs the distance r at $g_c = 3.045(2)$, which fits the scaling relation $G(r) \sim r^{-(1+\eta)} = r^{-1.036}$. Here, we also use the 3D Ising critical exponent $\eta = 0.036$, which corresponds to the black reference line. The scaling of $G(r)$ shows a power-law decay at the transition point.

As is shown in Fig. 7, the correlation function is always a constant in the FM Ising phase, in the dimer phase, or at the phase transition point. Its value is equal to 1 (blue line) only at the $k = (0, 0)$ momentum point [77] and is 0 anywhere else (red line). In the real space, all the imaginary time correlations $G_i(\tau) = \langle S_i^z(\tau) S_i^z(0)\rangle_{\mathrm{EH}}$ of site i are always A. All these pieces of evidence demonstrate that the EH must be a diagonal matrix in the S^z basis, which means that it is indeed a classical Ising model without any quantum fluctuation. It is definitely a nontrivial phenomenon that such a classical model emerges in the quantum entanglement.

Back to the effective Hamiltonian of a single layer, it seems like an Ising Hamiltonian with the quantum fluctuation term S_i^x on every site i. As shown in Fig. 8, a configuration of the path integral inside the RDM ρ_A contains several off-diagonal operators of the Heisenberg interaction which flip the spins along the time evolution. Because $(S_{A,i}^+ S_{B,i}^- + S_{A,i}^- S_{B,i}^+)$ acts on the interlayer, it takes an effective operator $(S_i^+ + S_i^-) \sim S_i^x$ on position i for a single layer A. Therefore the effective Hamiltonian of one layer has quantum fluctuations, which is truly different from the single-layer EH obtained from the above imaginary time correlations. In addition, there is a qualitative analogy: When the Heisenberg interaction is strong, the effective S_i^x term on subsystem A also becomes strong. The dimerized phase of the total system can be seen as a paramagnetic phase of subsystem A in this sense.

Finally, we find the explanation from the path integral of the RDM. As the EH is diagonal, it could be inferred that the RDM ρ_A is diagonal, and we can focus on proving that $\rho_A = \mathrm{Tr}_B(\rho)$ is diagonal. In our bilayer case, all the off-diagonal operators are from the Heisenberg interactions which act on the interlayer bonds only. To obtain ρ_A, we have to trace layer B, which is regarded as the environment. The trace operator requires the boundary condition of imaginary time to be periodic, which means that the off-diagonal operators should act an even number of times in layer B to keep the upper and lower spin configurations the same, as shown in Fig. 8. Therefore the off-diagonal operators must also act on layer A an even number of times to ensure that the RDM ρ_A is diagonal; that is, the upper and lower spin configurations of A should be the same as well.

Perhaps the reader thinks the above explanation is very tricky and dependent on the detailed QMC method. In fact, it is just based on a path-integral frame generally. $\rho_A = \mathrm{Tr}_B\{e^{-\beta H}\}$ is the definition of the RDM, and it can be rewritten via Taylor series expansion as $\mathrm{Tr}_B\{a_0 + a_1 H + a_2 H^2 + \cdots + a_n H^n\}$. The trace B requires that the initial and final configurations (bra and ket) of B should be the same. This means that the off-diagonal H operators should not change the initial configuration of B an odd number of times. In our case, all the off-diagonal operators act on both A and B; that is, the number of off-diagonal operators must be even. Because the off-diagonal operators work as $S_A^+ S_B^- + \mathrm{H.c.}$, this means that the initial configurations of A and B should be flipped the same number of times. Therefore the A configurations also stay unchanged. Furthermore, this conclusion can be generalized to more normal cases: All the intrasystem and intraenvironment interactions are diagonal, while the off-diagonal interactions only exist in the entangled boundary region.

Although the EH is always classical in these conditions, the EH levels become higher while the interlayer coupling interaction increases. Because the EE defined as $S_A =$

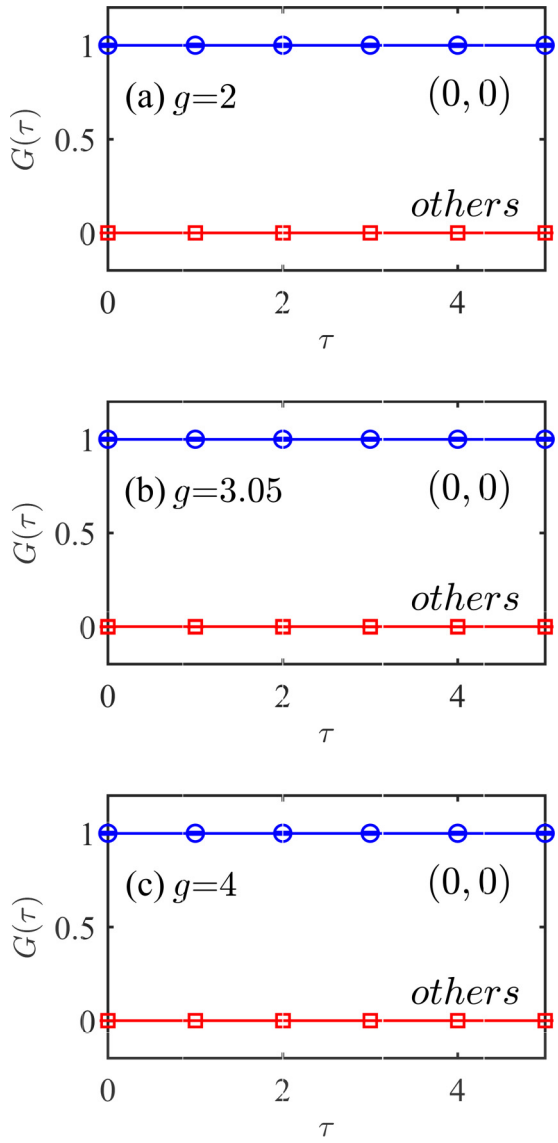

FIG. 7. $G(\tau)$ of the entanglement Hamiltonian in the momentum space of (a) the FM Ising phase, (b) the critical point, and (c) the dimerized phase. $G(\tau)$ at the Γ point (blue) and other momentum points (red) are calculated with different g. We find that $G(\tau)$ never decay in any phase, which is equal to 1 only at the (0,0) point and 0 at other momentum points.

$-\mathrm{Tr}(\rho_A \ln \rho_A)$ increases as the eigenlevels of the EH, the classical EH is consistent with the strong EE. In fact, for a real direct-product state without entanglement, its RDM is still a pure state, and the EH only has one level, which means there is no entanglement.

V. CONCLUSION

In this paper, we study a bilayer spin-$\frac{1}{2}$ model with intralayer FM Ising interaction and interlayer antiferromagnetic Heisenberg interaction. An efficient cluster update of SSE is developed to overcome the bounce problem [78] in the directed-loop update in pure Ising interactions. Using this developed QMC method, we determine the critical point

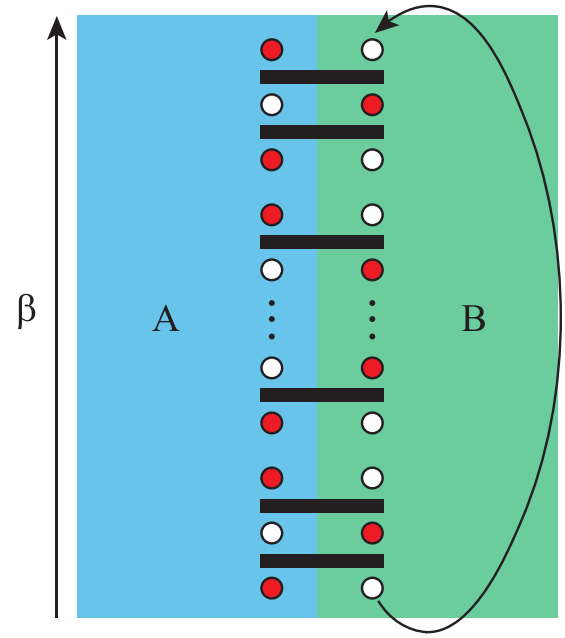

FIG. 8. Schematic diagram of the path integral of the RDM ρ_A in the SSE framework. The imaginary time boundary of the B part is periodic because of the $\mathrm{Tr}_B(\rho)$. The red (white) circles correspond to spin up (down). The horizontal black bars depict off-diagonal operator an off-diagonal operator. A (B) refers to the layer A (B). For convenience, we only draw one spin to represent one layer.

$g_c = 3.045(2)$ for the phase transition between the FM phase and the dimerized phase. Moreover, analysis of the critical exponents indicates that the phase transition belongs to the 3D Ising universality class.

Furthermore, we find that the quantum entanglement Hamiltonian of a single layer is a pure classical Ising model without any quantum fluctuation, although its effective Hamiltonian seems like a transverse-field Ising model. Therefore we give a more general conclusion for the reason why a classical entanglement Hamiltonian can emerge. By calculating the imaginary time correlations of the EH, we find that the EH is diagonal in both the FM phase and the dimerized phase, which can be explained by the path integral of the RDM.

ACKNOWLEDGMENTS

We thank Chang-Qin Wu, Bin-Bin Chen, and Zi Yang Meng for helpful discussions. We acknowledge the support from Zhejiang Provincial Natural Science Foundation of China under Grant No. LZ23A040003. Q.-F.L. acknowledges financial support of the MERIT-WINGS course provided by the University of Tokyo, and the Fellowship for Integrated Materials Science and Career Development provided by the Japan Science and Technology Agency. Y.-C.W. and S.W. thank Beihang Hangzhou Innovation Institute Yuhang for support. The numerical calculations in this paper have received support from the supercomputing system at the High-Performance Computing Centre of Beihang Hangzhou

Innovation Institute Yuhang. S.W. and B.-B.M. acknowledge Beijng Paratera Tech [79] for providing high-performance computing resources that have contributed to the research results reported in this paper.

[1] G. Vidal, J. I. Latorre, E. Rico, and A. Kitaev, Phys. Rev. Lett. **90**, 227902 (2003).
[2] V. E. Korepin, Phys. Rev. Lett. **92**, 096402 (2004).
[3] A. Kitaev and J. Preskill, Phys. Rev. Lett. **96**, 110404 (2006).
[4] M. Levin and X.-G. Wen, Phys. Rev. Lett. **96**, 110405 (2006).
[5] P. Calabrese and A. Lefevre, Phys. Rev. A **78**, 032329 (2008).
[6] E. Fradkin and J. E. Moore, Phys. Rev. Lett. **97**, 050404 (2006).
[7] Z. Nussinov and G. Ortiz, Proc. Natl. Acad. Sci. USA **106**, 16944 (2009).
[8] Z. Nussinov and G. Ortiz, Ann. Phys. (Amsterdam) **324**, 977 (2009).
[9] H. Casini and M. Huerta, Nucl. Phys. B **764**, 183 (2007).
[10] W. Ji and X.-G. Wen, Phys. Rev. Res. **1**, 033054 (2019).
[11] W. Ji and X.-G. Wen, Phys. Rev. Res. **2**, 033417 (2020).
[12] L. Kong, T. Lan, X.-G. Wen, Z.-H. Zhang, and H. Zheng, Phys. Rev. Res. **2**, 043086 (2020).
[13] X.-C. Wu, W. Ji, and C. Xu, J. Stat. Mech.: Theory Exp. (2021) 073101.
[14] X.-C. Wu, C.-M. Jian, and C. Xu, SciPost Phys. **11**, 033 (2021).
[15] J. Zhao, Y.-C. Wang, Z. Yan, M. Cheng, and Z. Y. Meng, Phys. Rev. Lett. **128**, 010601 (2022).
[16] J. Zhao, B.-B. Chen, Y.-C. Wang, Z. Yan, M. Cheng, and Z. Y. Meng, npj Quantum Mater. **7**, 69 (2022).
[17] Y.-C. Wang, N. Ma, M. Cheng, and Z. Y. Meng, SciPost Phys. **13**, 123 (2022).
[18] H. Li and F. D. M. Haldane, Phys. Rev. Lett. **101**, 010504 (2008).
[19] R. Thomale, D. P. Arovas, and B. A. Bernevig, Phys. Rev. Lett. **105**, 116805 (2010).
[20] D. Poilblanc, Phys. Rev. Lett. **105**, 077202 (2010).
[21] F. Pollmann, A. M. Turner, E. Berg, and M. Oshikawa, Phys. Rev. B **81**, 064439 (2010).
[22] L. Fidkowski, Phys. Rev. Lett. **104**, 130502 (2010).
[23] H. Yao and X.-L. Qi, Phys. Rev. Lett. **105**, 080501 (2010).
[24] E. Canovi, E. Ercolessi, P. Naldesi, L. Taddia, and D. Vodola, Phys. Rev. B **89**, 104303 (2014).
[25] D. J. Luitz, F. Alet, and N. Laflorencie, Phys. Rev. Lett. **112**, 057203 (2014).
[26] D. J. Luitz, F. Alet, and N. Laflorencie, Phys. Rev. B **89**, 165106 (2014).
[27] D. J. Luitz, N. Laflorencie, and F. Alet, J. Stat. Mech.: Theory Exp. (2014) P08007.
[28] C.-M. Chung, L. Bonnes, P. Chen, and A. M. Läuchli, Phys. Rev. B **89**, 195147 (2014).
[29] H. Pichler, G. Zhu, A. Seif, P. Zoller, and M. Hafezi, Phys. Rev. X **6**, 041033 (2016).
[30] J. I. Cirac, D. Poilblanc, N. Schuch, and F. Verstraete, Phys. Rev. B **83**, 245134 (2011).
[31] V. M. Stojanović, Phys. Rev. B **101**, 134301 (2020).
[32] W.-z. Guo, J. High Energy Phys. 02 (2021) 085.
[33] T. Grover, Phys. Rev. Lett. **111**, 130402 (2013).
[34] F. F. Assaad, T. C. Lang, and F. Parisen Toldin, Phys. Rev. B **89**, 125121 (2014).
[35] F. F. Assaad, Phys. Rev. B **91**, 125146 (2015).
[36] F. Parisen Toldin and F. F. Assaad, Phys. Rev. Lett. **121**, 200602 (2018).
[37] X.-J. Yu, R.-Z. Huang, H.-H. Song, L. Xu, C. Ding, and L. Zhang, Phys. Rev. Lett. **129**, 210601 (2022).
[38] C. Kokail, R. van Bijnen, A. Elben, B. Vermersch, and P. Zoller, Nat. Phys. **17**, 936 (2021).
[39] Z. Yan and Z. Y. Meng, arXiv:2112.05886.
[40] A. I. Liechtenstein, I. I. Mazin, and O. K. Andersen, Phys. Rev. Lett. **74**, 2303 (1995).
[41] M. Golor, T. Reckling, L. Classen, M. M. Scherer, and S. Wessel, Phys. Rev. B **90**, 195131 (2014).
[42] T. Dahm, D. Manske, and L. Tewordt, Phys. Rev. B **54**, 6640 (1996).
[43] F. Forsthofer, S. Kind, and J. Keller, Phys. Rev. B **53**, 14481 (1996).
[44] L. Wang, K. S. D. Beach, and A. W. Sandvik, Phys. Rev. B **73**, 014431 (2006).
[45] G. Trambly de Laissardière, D. Mayou, and L. Magaud, Nano Lett. **10**, 804 (2010).
[46] G. Trambly de Laissardière, D. Mayou, and L. Magaud, Phys. Rev. B **86**, 125413 (2012).
[47] R. Bistritzer and A. H. MacDonald, Proc. Natl. Acad. Sci. USA **108**, 12233 (2011).
[48] A. Rozhkov, A. Sboychakov, A. Rakhmanov, and F. Nori, Phys. Rep. **648**, 1 (2016).
[49] J. M. B. Lopes dos Santos, N. M. R. Peres, and A. H. Castro Neto, Phys. Rev. Lett. **99**, 256802 (2007).
[50] J. M. B. Lopes dos Santos, N. M. R. Peres, and A. H. Castro Neto, Phys. Rev. B **86**, 155449 (2012).
[51] B. A. Bernevig, Z.-D. Song, N. Regnault, and B. Lian, Phys. Rev. B **103**, 205413 (2021).
[52] Y. Da Liao, Z. Y. Meng, and X. Y. Xu, Phys. Rev. Lett. **123**, 157601 (2019).
[53] B.-B. Chen, Y. D. Liao, Z. Chen, O. Vafek, J. Kang, W. Li, and Z. Y. Meng, Nat. Commun. **12**, 5480 (2021).
[54] Y.-C. Wang, Z. Yan, C. Wang, Y. Qi, and Z. Y. Meng, Phys. Rev. B **103**, 014408 (2021).
[55] X. Zhang, G. Pan, Y. Zhang, J. Kang, and Z. Y. Meng, Chin. Phys. Lett. **38**, 077305 (2021).
[56] G. Pan, X. Zhang, H. Li, K. Sun, and Z. Y. Meng, Phys. Rev. B **105**, L121110 (2022).
[57] X. Zhang, K. Sun, H. Li, G. Pan, and Z. Y. Meng, Phys. Rev. B **106**, 184517 (2022).
[58] O. F. Syljuåsen and A. W. Sandvik, Phys. Rev. E **66**, 046701 (2002).
[59] A. W. Sandvik, Phys. Rev. Lett. **104**, 177201 (2010).
[60] A. W. Sandvik and J. Kurkijärvi, Phys. Rev. B **43**, 5950 (1991).
[61] A. W. Sandvik, Phys. Rev. B **59**, R14157 (1999).
[62] A. W. Sandvik, Phys. Rev. E **68**, 056701 (2003).
[63] Prof. Sandvik provides open-source code and a tutorial at http://physics.bu.edu/~sandvik/programs/ssebasic/ssebasic.html.
[64] Z. Yan, Y. Wu, C. Liu, O. F. Syljuåsen, J. Lou, and Y. Chen, Phys. Rev. B **99**, 165135 (2019).

[65] Z. Yan, Phys. Rev. B **105**, 184432 (2022).
[66] A. W. Sandvik, in *Lectures on the Physics of Strongly Correlated Systems XIV: Fourteenth Training Course in the Physics of Strongly Correlated Systems*, AIP Conference Proceedings Vol. 1297 (American Institute of Physics, College Park, MD, 2010), p. 135.
[67] Z. Yan, L. Pollet, J. Lou, X. Wang, Y. Chen, and Z. Cai, Phys. Rev. B **97**, 035148 (2018).
[68] Z. Zhou, C. Liu, D.-X. Liu, Z. Yan, Y. Chen, and X.-F. Zhang, SciPost Phys. **14**, 037 (2023).
[69] Z. Zhou, C. Liu, Z. Yan, Y. Chen, and X.-F. Zhang, npj Quantum Mater. **7**, 60 (2022).
[70] Z. Zhou, Z. Yan, C. Liu, Y. Chen, and X.-F. Zhang, arXiv:2106.05518.
[71] K. Binder, Phys. Rev. Lett. **47**, 693 (1981).
[72] K. Binder, Z. Phys. B: Condens. Matter **43**, 119 (1981).
[73] K. Binder and D. P. Landau, Phys. Rev. B **30**, 1477 (1984).
[74] A. Pelissetto and E. Vicari, Phys. Rep. **368**, 549 (2002).
[75] H. Kleinert, Phys. Rev. D **60**, 085001 (1999).
[76] M. E. Fisher and M. N. Barber, Phys. Rev. Lett. **28**, 1516 (1972).
[77] Because the A part still has periodic boundary conditions even if tracing out the B part, we can well define the momentum basis in this case. We can rewrite the Hamiltonian from the real space into the momentum space through a Fourier transform. In fact, this means we use the momentum basis $|S^z_k\rangle$ instead of the real space basis $|S^z_i\rangle$. Figure 7 shows the imaginary time correlation function of momentum space which can be obtained from real space correlations via Fourier transform, that is, $C(k) = \sum_r e^{-kr} C(r)$. Because here A is a 2D system, k and r are also 2D, $r = (i, j)$ with $i, j = 0, 1, \ldots, L-1$ and $k = 2\pi/L(m, n)$ with $m, n = 0, 1, \ldots, L-1$.
[78] When we use the directed-loop update to sample the QMC configurations, if the S^zS^z term is much larger than the $S^+S^- + \text{H.c.}$ term, the update lines will always go back (bounce) when they meet the vertex. This makes the samplings very ineffective. Thus strong Ising interactions usually lead to a hard simulation for the QMC method.
[79] https://www.paratera.com/.